Terahertz responses of the high-temperature metallic phase and photoinduced metallic state in the ferroelectric charge-ordered organic salt α-$(ET)_2I_3$

H. Nakaya,[1] K. Itoh,[1] Y. Takahashi,[1] H. Itoh,[1,2] S. Iwai,[1,2,*] S. Saito,[3] K. Yamamoto,[4] and K. Yakushi[4]
[1]*Department of Physics, Tohoku University, Sendai 980-8578, Japan*
[2]*JST, CREST, Sendai 980-8578, Japan*
[3]*National Institute of Information and Communications Technology, Kobe 651-2492, Japan*
[4]*Institute for Molecular Science, Okazaki 444-8585, Japan*
(Received 19 September 2009; revised manuscript received 24 January 2010; published 14 April 2010)

The thermal and photoinduced phase transitions between the ferroelectric charge-ordered (CO) insulator state and the metallic state in the layered organic salt α-$(ET)_2I_3$ (ET: [bis(ethylenedithio)]-tetrathiafulvalene) were investigated using terahertz time-domain spectroscopy. Characteristic increases were observed in the optical conductivity and the dielectric constant upon increasing the temperature to just below the insulator-to-metal transition temperature (T_{CO}), which reflects the partial or precursory collapse of the ferroelectric state and charge ordering. The excitation of this partially melted CO state near T_{CO} led to the formation of a photoinduced macroscopic metallic state, whose conductivity appeared to be greater than that of a high-temperature metallic state. At $T \ll T_{CO}$, a microscopic metallic state was formed within the rigid CO state.

DOI: 10.1103/PhysRevB.81.155111 PACS number(s): 71.30.+h, 74.70.Kn, 78.30.Jw

I. INTRODUCTION

Low-dimensional organic conductors exhibit various electronic states such as the charge-ordered (CO) insulator, Mott insulator, metallic, and superconducting states because of strong on-site and/or intersite Coulomb repulsion.[1–5] Among these states, metallic states are of great interest because they sometimes exhibit characteristics that differ greatly from those of a Fermi-liquid metal. The electronic properties of such metallic states are related to the mechanisms of the insulator-to-metal (*I-M*) transition and the formation of the ferroelectric state.

The layered organic salt α-$(ET)_2I_3$ (ET: [bis(ethylenedithio)]-tetrathiafulvalene)] (Refs. 6–19) is a typical three-quarter-filled organic conductor. However, this compound is a CO insulator that exhibits electron ferroelectricity at temperatures lower than the metal-insulator transition temperature (T_{CO}=135 K). It is noteworthy that the compound is ferroelectric not because of structural deformation but because of the long-range order of the charge disproportionation (CD) in the CO insulator.[16] Such ferroelectric characteristics have also been detected in major quasi-one-dimensional bis-tetramethyl-tetrathiafulvalene (TMTTF) salt[3–5,20] and other layered organic salts.[21,22] The CO state can transform to a high-temperature (HT) metallic state, as shown schematically in Fig. 1. However, the HT metallic state does not exhibit a Drude response but displays characteristics of semimetals and narrow (zero)-gap semiconductors.[7,14,15] As shown in the inset of Fig. 1, the CO insulator–HT metallic state transition (hereinafter referred to as the CO-HT transition) is well reflected by the optical conductivity spectra in the midinfrared (mid-IR) and terahertz (THz) regions.[17–19] Moreover, microwave conductivity measurements have indicated marked changes in the conducting nature at $T=T_{CO}$ and even at $T<T_{CO}$.[6] However, detailed spectral changes in the THz region reflecting the phase transition from the CO ferroelectric state to the HT metallic state near T_{CO} have not yet been clarified.

Recently, layered ET salts have shown a potential for application to ultrafast optical switching devices.[16,23–27] The ultrafast optical response is ascribed to the photoinduced *I-M* transition (PIMT). The time evolution of the transient reflectivity of α-$(ET)_2I_3$ in the mid-IR region suggests the formation of quasistable macroscopic ($T \sim T_{CO}$) and short-lived microscopic ($T \ll T_{CO}$) metallic states.[24,25] However, the spectroscopic characterization of these microscopic and macroscopic states has not been performed.

In this paper, the thermal CO-HT transition and the PIMT in α-$(ET)_2I_3$ are investigated using THz time-domain spectroscopy. Characteristic increases in the real parts of the steady-state optical conductivity (σ_1) and dielectric constant (ε_1) are observed upon increasing the temperature to just below T_{CO}, in terms of the partial or precursory collapse of

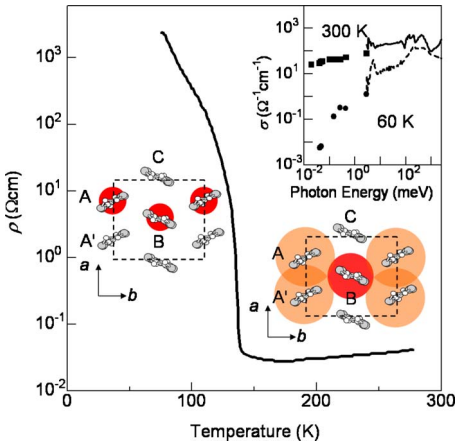

FIG. 1. (Color online) Temperature dependence of resistivity (Ref. 15) and molecular arrangement of α-$(ET)_2I_3$. In the CO state, electrons are localized as illustrated by the red circles. However, they are extended as shown by the orange circles in the *A*-*A*′ stack in the HT metallic state (but they are not so extended in the *B*-*C* stack) (Ref. 12). The inset shows the optical conductivity spectra at 300 K (metallic) and 60 K (CO) (Refs. 18 and 19).

the ferroelectric state and charge ordering. Optical pump-THz probe (transient absorption) measurements show that the optical excitation of the ferroelectric CO state, which melted partially near T_{CO}, results in the photoinduced formation of a quasistable macroscopic metallic state, although the unstable microscopic metallic state is formed in the rigid CO state at $T \ll T_{CO}$.

II. EXPERIMENT

Single crystals of α-$(ET)_2I_3$ (average size: $2\times2\times0.05$ mm^3) were prepared using a previously reported procedure.[7] The steady-state spectra of the optical conductivity (σ_1) and the dielectric constant (ε_1) of the crystals were obtained in the energy range of 2–15 meV (0.5–4 THz) using a THz time-domain spectrometer (Rayfact SpecTera RS-01020; Tochigi Nikon). The crystals were contained in a cryostat and the temperature was varied from 7 to 300 K.

Near-infrared (NIR) pump (0.89 eV)-THz-probe (1.5–10 meV) spectroscopy was performed using a 1-kHz Ti:Al_2O_3 regenerative amplifier system (Hurricane; Spectra-Physics) as the light source. The output of the amplifier was divided into three beams. The first beam was used to generate the NIR pump pulses in a handmade optical parametric amplifier, and the second to generate the THz probe pulses. The THz pulses were generated by difference-frequency generation in a ZnTe crystal with dimensions of $20\times20\times1$ mm^3 and were focused on a single crystal of α-$(ET)_2I_3$ in a 1.5-mm-diameter region excited by the pump beam. The third beam was used for electro-optic (EO) sampling, which was performed to detect the THz light transmitted through the sample. The time resolution was approximately 1 ps. The time delay between the NIR pump pulse and the THz probe pulse (t_d) and that between the THz probe pulse and the gate pulse (t_g) were varied using computer-controlled stepping motors.

III. RESULTS AND DISCUSSION

A. Steady-state phase transition

Figure 2(a) shows time profiles of the transmitted electric field ($E_{TH}\|b$) at 7 and 150 K. $\sigma_1(\omega)$ and $\varepsilon_1(\omega)$ are obtained from the time profiles of E_{TH} for various temperatures, as shown in Figs. 2(b) and 2(c). At a low temperature (7 K), $\sigma_1(\omega)$ is small ($\sigma_1<2$ Ω^{-1} cm^{-1}), which reflects the insulating nature of α-$(ET)_2I_3$. Low-frequency phonon structures are also detected at 5.2, 6.6, 8.6, 11.8, 13.0, and 15.5 meV in both the $\sigma_1(\omega)$ and $\varepsilon_1(\omega)$ spectra. Such low-frequency phonons might be attributed to the ET libration or the I_3 stretching mode.[28] An abrupt increase in σ_1 and a decrease in ε_1 with an increase in temperature at T_{CO} indicate the CO-HT transition. The absolute value of σ_1 at 3 meV and the overall spectral features of $\sigma_1(\omega)$ and $\varepsilon_1(\omega)$ are roughly consistent with previously reported dc conductivity measurements (approximately 30 Ω^{-1} cm^{-1}) (Refs. 7, 14, and 15) and IR spectra,[18,19] respectively. However, $\varepsilon_1(\omega)$ in the metallic phase ($T>T_{CO}$) does not exhibit a Drude-like negative response. Considering that the THz optical conductivity and the dc conductivity for $T>T_{CO}$ are much less than that for a

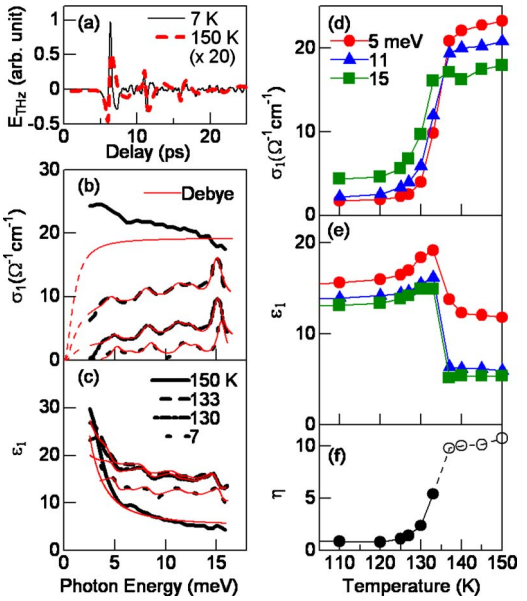

FIG. 2. (Color online) (a) THz profiles in time domain at 7 and 150 K (×20) for $E_{TH}\|b$. [(b) and (c)] σ_1 and ε_1 at various temperatures. The red (gray) curves indicate the values calculated using the equation given in the text. [(d) and (e)] Temperature dependence of σ_1 and ε_1 at 5 meV [solid red (gray) circles], 11 meV [solid blue (gray) triangles], and 15 meV [green (gray) squares]. (f) Temperature dependence of η ($T<T_{CO}$) (solid black circles and solid curve). For $T>T_{CO}$, η is indicated by the open circles and the dashed curve because the $\sigma_1(\omega)$ spectra cannot be well reproduced.

Fermi-liquid-like metal (such as the metallic phase in κ-$(ET)_2X$ at low temperature[29,30]), a possible explanation of such a low σ_1 and a positive ε_1 is the existence of a narrow (zero)-gap semiconductor state.[14,15]

Figures 2(d) and 2(e) show the temperature dependence of $\sigma_1(\omega)$ and $\varepsilon_1(\omega)$ at 5, 11, and 15 meV. It is noteworthy that $\sigma_1(\omega)$ and $\varepsilon_1(\omega)$ start to increase with increasing temperature at ~120 K, which is below T_{CO}. This behavior indicates a decrease in the optical gap to below 15 meV for 120 K $<T<T_{CO}$. For both 120 K$<T<T_{CO}$ and $T>T_{CO}$, the spectral shape of $\sigma_1(\omega)$ and $\varepsilon_1(\omega)$ cannot be explained using the Drude model. The gradual closing of the gap has already been suggested by microwave conductivity measurements.[6] Considering that the ferroelectric state is formed because of charge ordering, the growth in $\sigma_1(\omega)$ and $\varepsilon_1(\omega)$ with an increase in temperature for 120 K$<T<T_{CO}$ is attributable to the partial or precursory collapse of the ferroelectric state and charge ordering, indicating that formation of the relaxerlike state (i.e., fluctuations in the long-range order of the CD near T_{CO}) results in an increase in ε_1.

In this paper, we phenomenologically analyzed the observed $\sigma_1(\omega)$ and $\varepsilon_1(\omega)$ by using the Debye model for partially melted CO ferroelectric states and the Lorentz model for phonons, respectively. We assumed that $\sigma_1(\omega)$ and $\varepsilon_1(\omega)$ include contributions from charges [$\sigma_e(\omega)$ and $\varepsilon_e(\omega)$] and phonons [$\sigma_v(\omega)$ and $\varepsilon_v(\omega)$], respectively;

$$\sigma_1 = \sigma_e + \sigma_v, \quad \varepsilon_1 = \varepsilon_e + \varepsilon_v, \tag{1}$$

TABLE I. Phonon parameters ξ_i, ω_{i0}, and τ_{vi} for $i=1,2,\ldots,6$ at 7 K.

i	ξ_i (s^{-2})	ω_{i0} (meV)	τ_{vi} (ps)
1	3.35×10^{24}	5.2	0.53
2	1.24×10^{24}	6.6	0.53
3	5.29×10^{24}	8.6	0.41
4	4.59×10^{24}	11.8	0.41
5	2.29×10^{24}	13.0	0.53
6	7.77×10^{24}	15.5	0.66

$$\sigma_e(\omega)=\eta\frac{\omega^2\tau}{1+\omega^2\tau^2},\quad \varepsilon_e(\omega)=\varepsilon(\infty)+4\pi\eta\frac{1}{1+\omega^2\tau^2},\quad (2)$$

$$\sigma_v(\omega)=\sum_i\frac{\xi_i\omega}{(\omega_{i0}^2-\omega^2)^2+(\omega/\tau_{vi})^2},\quad \varepsilon_v(\omega)=\varepsilon_{v0}+\sum_i\frac{\xi_i(\omega_{i0}^2-\omega^2)}{(\omega_{i0}^2-\omega^2)^2+(\omega/\tau_{vi})^2}.\quad (3)$$

In these equations, $\eta=ne^2\tau^2f/m$, where n, e, τ, m, and f represent the density, elemental charge, damping time, effective mass, and carrier oscillator strength, respectively. ξ_i are phonon parameters that are determined by phonon density, effective mass, and effective charge of the respective phonon peaks i. We employed the Debye model to analyze the partially melted CO insulating state for $T<T_{CO}$, but not to reproduce the metallic state for $T>T_{CO}$. In fact, for $T<T_{CO}$, $\sigma_1(\omega)$ and $\varepsilon_1(\omega)$ can be well reproduced using the above equations, as shown by the red curves in Figs. 2(b) and 2(c). For $T>T_{CO}$, however, the observed spectra cannot be represented by the Debye model because the additional metallic component emerges below 5 meV.

The temperature dependence of η is shown in Fig. 2(f) by solid circles joined by a solid curve for $T<T_{CO}$ but is indicated by the open circles joined by the dashed curve for $T>T_{CO}$ because the $\sigma_1(\omega)$ spectra cannot be well reproduced. The quantities η and τ are determined by the fitting procedure to be 5.4 and 0.53 ps, respectively, at 133 K ($<T_{CO}$). If we assume $m=9.1\times10^{-28}$ g and $f=0.1$, then n is estimated to be 4.6×10^{-17} cm^{-3} although the parameters n, m, and f cannot be determined independently.

The damping energy $\hbar/\tau=8.1$ meV is roughly consistent with the energy scale of the corresponding temperature ($\sim$100 K). The phonon parameters ξ_i, ω_{i0}, and τ_{vi} for $i=1,2,\ldots,6$ at 7 K are listed in Table I. These phonons will be assigned and discussed in more detail in future studies because this is not the focus of the present study.

Thus, the small-gap state that reflects the partial collapse of the ferroelectric state and charge ordering at 120 K$<T<T_{CO}$ is described by the Debye model. However, another low-energy spectral component in $\sigma_1(\omega)$ is observed at $T>T_{CO}$, which suggests that $\sigma_1(0)>0$. This observation is consistent with the abrupt increase in the dc conductivity at T_{CO}. The abrupt disappearance of the phonon structure as T exceeds T_{CO} indicates dielectric screening of the phonons.

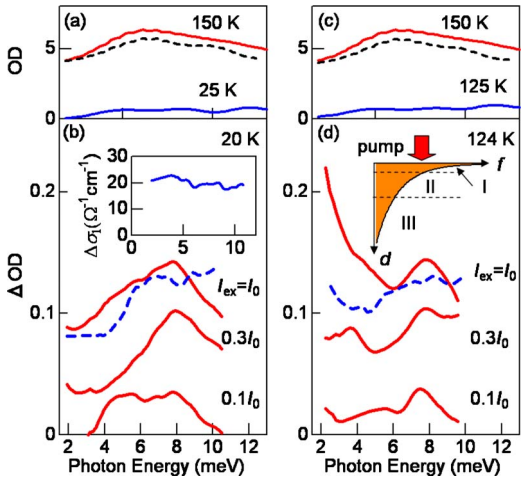

FIG. 3. (Color online) [(a) and (c)] Absorption (OD) spectra of CO and HT phases for $E_{TH}\|b$ at 25 K [CO, blue (gray)], 125 K [CO, blue (gray)], and 150 K [HT metallic state, red (gray)]. Dashed curves in (a) and (c) indicate the differential spectra for [OD(150 K)-OD(25 K)] and [OD(150 K)-OD(125 K)], respectively. [(b) and (d)] Transient absorption (ΔOD) spectra under excitation (polarization of the pump light $E\|b$) at 0.89 eV at 20 and 124 K, respectively, for various excitation intensities I_{ex}. The blue dashed curves indicate the spectra determined using the multilayer model (see the text). The inset of (b) shows photoinduced changes in σ ($\Delta\sigma$), which are calculated using the multilayer model. The density of the photoinduced conducting state (f) is shown schematically as a function of d in the inset of (d).

Therefore, the thermal CO-HT transition occurs in the following manner. First, for 120 K$<T<T_{CO}$, the optical gap gradually decreases with increasing temperature. The small-gap state, which can be represented by the Debye model, reflects the partial or precursory collapse of the ferroelectric state and charge ordering. Second, for $T=T_{CO}$, the metallic state, which is characterized by the low-energy spectral component $\sigma_1(0)>0$, abruptly appears and the low-frequency phonons are screened as the temperature increases. The temperature dependence of the conducting nature for $T<T_{CO}$ has been reported previously.[6] Our THz spectroscopic study near T_{CO} shows that this characteristic temperature dependence is attributable to the partial collapse of the ferroelectric state and charge ordering.

B. Photoinduced phase transition

Next, the electronic properties of the photoinduced metallic state are discussed on the basis of the transient absorption spectra (ΔOD, where OD is the optical density).[31] Figures 3(a) and 3(c) show the absorption spectra of the CO and HT metallic states of α-$(ET)_2I_3$, respectively, for polarization parallel to the b axis at 25 K (rigid CO state), 125 K (partially melted CO state or, equivalently, the small-gap state), and 150 K (HT state). In Figs. 3(b) (20 K) and Fig. 3(d) (124 K), ΔOD spectra are presented for a pump-probe time delay of $t_d=0.1$ ps (polarization of the pump light $E\|b$) at

0.89 eV for various values of excitation intensity I_{ex} (I_0 =0.01 mJ cm^{-2}). The broad absorption increase is induced by photoexcitation in the THz region at 20 K, which suggests the formation of the metallic state. The spectral shape of ΔOD measured at 20 K is analogous to the temperature differential spectrum, i.e., OD(150 K)–OD(25 K) [indicated by the dashed curve in Fig. 3(a)], whereas ΔOD at 124 K is different from OD(150 K)–OD(125 K) [indicated by the dashed curve in Fig. 3(c)]. These results indicate that the photoinduced metallic state at 20 K is similar to the HT metallic state, whereas that at 124 K is different from the HT metallic state.[31]

The magnitude of the photoinduced absorption change (ΔOD=0.15 at 8 meV for $I_{ex}=I_0$) is much less than that for the thermal CO-HT transition [OD(150 K)−OD(25 K)=4]. However, considering the large difference between the penetration depth of the NIR pump and that of the THz probe, the magnitude of the absorption change in the surface layer is expected to be as large as that for the thermal CO-HT transition. This is confirmed through analyses using the multilayer model, which will be discussed later. It is noteworthy that the ΔOD spectrum at 124 K is markedly different from that at 20 K. Put more precisely, the low-energy (<5 meV) ΔOD spectrum at 124 K for $I_{ex}=I_0$ is larger than that at 20 K, which shows the different nature of the photoinduced metallic state at 20 K compared with that at 124 K. Nevertheless, further investigation is necessary to confirm this rationale because the inhomogeneity of the photoinduced metallic state affects the shape of the ΔOD spectrum.

The ΔOD spectrum can be obtained using the multilayer model if the complex dielectric function of the photoinduced metallic state is described by that of the HT metallic phase. It is reasonable to consider that the density f of a spherical photoinduced metallic state with a diameter r, which is considerable less than THz wavelengths, decreases as a function of the distance d from the surface. The density can thus be represented by $f(d)=\exp(-\alpha d)$, where α is the absorption coefficient at the excitation wavelength ($\alpha=1\times10^4$ cm^{-1}), as shown in the schematic of Fig. 3(d). The complex effective dielectric constants ε_{eff} of the different layers are then described by effective-medium theory[32–34] as $(\varepsilon_{eff}-\varepsilon_I)/(\varepsilon_{eff}+2\varepsilon_I)=(1-f)(\varepsilon_M-\varepsilon_I)/(\varepsilon_M+2\varepsilon_I)$ for $0.7<f<1$ (the Maxwell–Garnett equation for the surface region I), $f(\varepsilon_{eff}-\varepsilon_I)/\varepsilon_M+2\varepsilon_I(\varepsilon_M/\varepsilon_{eff})^{1/3}=(1-f)$ for $0.3<f<0.7$ (Hanai's equation for the intermediate region II), and $(\varepsilon_{eff}-\varepsilon_M)/(\varepsilon_{eff}+2\varepsilon_M)=f(\varepsilon_I-\varepsilon_M)/(\varepsilon_I+2\varepsilon_M)$ for $0<f<0.3$ (the Maxwell–Garnett equation for the deep region III), where ε_I and ε_M are the complex dielectric constants of the CO and the HT metallic phases, respectively.

The dashed curves in Figs. 3(b) and 3(d) indicate the ΔOD spectra obtained using the multilayer model. The calculated spectral shape and magnitude are approximately equivalent to those of the ΔOD spectrum observed at 20 K. The inset of Fig. 3(b) shows the photoinduced changes in $\sigma(\omega)$ [$\Delta\sigma(\omega)$] of the surface layer in the multilayer model. The spectrum $\Delta\sigma(\omega)$ is roughly equivalent to that of $\sigma(\omega)$ for the HT metallic state, indicating that the electronic properties of the photoinduced metallic state at 20 K ($\ll T_{CO}$) are similar to those of the HT metallic state. However, the low-energy (<5 meV) absorption observed at 124 K appears to be larger than that of the HT metallic state [indicated by the dashed curve in Fig. 3(d)], which suggests that the photoinduced metallic state formed in the partially melted CO state is different from the HT metallic state. We consider the conductivity of the photoinduced metallic state at 124 K to be larger than that of the HT metallic state.

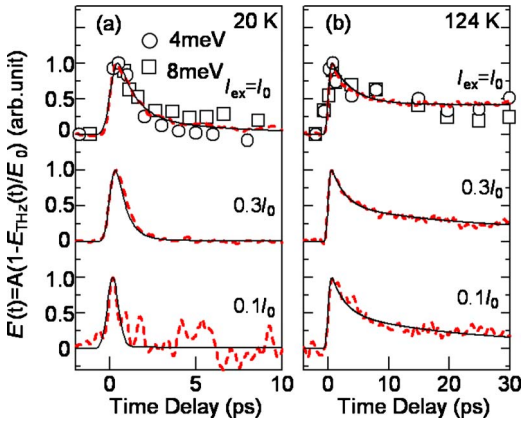

FIG. 4. (Color online) [(a) and (b)] Time evolution of ΔOD at 4 and 8 meV (open circles and squares) at 20 and 124 K, respectively. The red dashed curves indicate the time evolution of the normalized THz amplitude $E''(t)=A(1-E_{TH}(t)/E_0)$.

A difference in the decay time of the absorption change is discernible between the photoinduced metallic state observed at 20 K and that observed at 124 K. The time evolution of ΔOD at 20 K and at 124 K is shown in Figs. 4(a) and 4(b), respectively. The figures show data obtained at 4 and 8 meV, which are denoted by circles and squares, respectively. The dashed red curves show the time evolution of the photoinduced change in the transmitted THz amplitude E_{TH}. The quantity E_{TH} is normalized by E_0 in calculating the time evolution $E''(t)=A(1-E_{TH}(t)/E_0)$, where E_0 and A represent the amplitude before the photoexcitation and the normalizing coefficient, respectively. Because $E''(t)$ is similar to ΔOD(t), hereinafter, we use $E''(t)$ to evaluate the time evolution. The relaxation time of the HT metallic state is comparable to the time resolution (approximately 1 ps) at 20 K, although the photoinduced metallic state observed at 124 K shows a much longer decay time—of the order of nanoseconds. The decay time increases with increasing I_{ex}, which reflects the cooperative nature of the photoinduced metallic state.

The inset of Fig. 5 shows $E'(t)$ various temperatures $T<T_{CO}$. The decay time constants τ_{fast} and τ_{slow} are shown as a function of the reduced temperature $(T/T_{co}-1)$ by solid red diamonds in Fig. 5. The decay time constants are obtained by fitting the data to the sum of three exponential functions, which gives the results $\tau_{fast}\sim2$ ps, $\tau_{middle}\sim15$ ps, and $\tau_{slow}\sim1$ ns. Of the three components, τ_{middle}, whose fraction is approximately 5%, is independent of temperature, which indicates that it is unrelated to the *I-M* transition.[24,25] The time constant τ_{fast} dominates at 20 K, whereas the contribution of τ_{slow} becomes large at 124 K. Therefore, τ_{fast} and τ_{slow} correspond to the ΔOD spectra at 20 and 124 K, respectively. τ_{fast} and τ_{slow} are given by the expressions $\tau_{slow}\propto|T/T_C-1|^{1.8}$ and $\tau_{fast}\propto|T/T_C-1|^{0.5}$. We attribute the increase in the decay time at temperatures close to T_{CO} to critical slowing

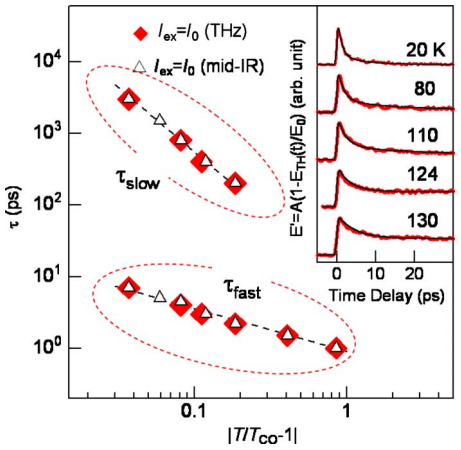

FIG. 5. (Color online) Decay time constants τ_{fast} and τ_{slow} [red (gray) diamonds] as functions of reduced temperature. The decay time constants obtained in a mid-IR pump-probe study are indicated by open triangles ($I_{ex}=I_0$) (Ref. 21). The inset shows $E(t)$ at various temperatures $T<T_{CO}$.

down (CSD), which reflects the statistical nature of the photoinduced metallic states. The CSD behavior, indicated by the open triangles ($I_{ex}=I_0$) in Fig. 5(b), has previously been observed in a mid-IR pump-probe study.[24,25] The time constants τ_{fast} and τ_{slow} correspond to different critical exponents (given by νz, where ν and z signify the critical exponent of the correlation length ξ and the dynamic critical exponent, respectively). A decay time of the order of nanoseconds and $\nu z=1.8$ for τ_{slow}, which is close to the value of 2.1665,[35,36] are obtained by using the two-dimensional Ising model and indicates the photoinduced formation of a quasistable macroscopic metallic state in the partially melted CO state at 124 K. This is consistent with the observation of a characteristic large low-energy absorption at 124 K, which reflects a metallic state with high conductivity. However, the short decay time (approximately 2 ps) of τ_{fast} indicates the formation of an unstable microscopic metallic state in the rigid CO state at 20 K. The electronic nature of the microscopic metallic state is similar to that of the HT metallic state.

The electronic properties of the photoinduced macroscopic metallic state remain unclear. However, one possible explanation is that in the photoinduced macroscopic metallic state, the CD is melted on the *B*-*C* molecular stacks (Fig. 1) arising from the asymmetric structure, is markedly weakened in addition to the melting of the correlated CD on the *A*-*A'* stack. In the HT metallic state, however, the CD on the *B*-*C* stack remains.[12,37]

In summary, we have investigated the THz response of the HT metallic state and a photoinduced metallic state in the ferroelectric CO organic salt α-$(ET)_2I_3$. The temperature dependence of the optical conductivity and of the dielectric constant shows the incomplete collapse of the ferroelectric state and charge ordering just below T_{CO}. The electronic nature of the photoinduced macroscopic metallic state formed at 124 K ($T\sim T_{CO}$) is different from the photoinduced microscopic metallic state observed at 20 K ($T\ll T_{CO}$). In other words, the quasistable macroscopic metallic state is formed in the partially melted CO state ($T\sim T_{CO}$), but an unstable microscopic metallic state is formed in the rigid CO state ($T\ll T_{CO}$). The measured low-energy (<5 meV) transient absorption spectra suggest that the conductivity of the photoinduced macroscopic metallic state is greater than that of the HT metallic state.

ACKNOWLEDGMENTS

We would like to thank K. Yonemitsu, S. Ishihara, A. Takahashi, H. Seo, T. Sasaki, and H. Kishida for their valuable discussions. This work was supported by a Grant-in-Aid for Scientific Research on Innovative Areas (New Frontier in Materials Science Opened by Molecular Degrees of Freedom, Grant No. 20110005) and another Grant-in-Aid (B, Grant No. 20340069) from the Ministry of Education, Science and Culture, Japan.

*s-iwai@m.tains.tohoku.ac.jp

[1] P. Batail, Chem. Rev. **104**, 4887 (2004).
[2] See the Special Topics section: Organic Conductors, edited by S. Kagoshima, K. Kanoda, and T. Mori, J. Phys. Soc. Jpn. **75**, 051001 (2006).
[3] *Physics of Organic Superconductors and Conductors*, Springer Series in Materials Sciences, Vol. 110, edited by A. G. Lebed (Springer, Berlin, 2008).
[4] *Proccedings of ECRAYS08*, edited by S. Brazovskii, N. Kirova, and P. Monceau [Physica B 404, 347 (2008)].
[5] F. Nad, P. Monceau, K. Hiraki, and T. Takahashi, J. Phys.: Condens. Matter **16**, 7107 (2004).
[6] K. Bender, K. Dietz, H. Endres, H. W. Helberg, I. Henning, H. J. Keller, H. W. Schafer, and D. Schweitzer, Mol. Cryst. Liq. Cryst. **107**, 45 (1984).
[7] K. Bender, I. Henning, D. Schweitzer, K. Dietz, H. Endres, and H. J. Keller, Mol. Cryst. Liq. Cryst. **108**, 359 (1984).
[8] J. Moldenhauer, Ch. Horn, K. I. Pokhodnia, and D. Schweitzer, Synth. Met. **60**, 31 (1993).
[9] H. Kino and H. Fukuyama, J. Phys. Soc. Jpn. **65**, 2158 (1996).
[10] Y. Takano, K. Hiraki, H. M. Yamamoto, T. Nakamura, and T. Takahashi, Synth. Met. **120**, 1081 (2001).
[11] R. Wojciechowski, K. Yamamoto, K. Yakushi, M. Inokuchi, and A. Kawamoto, Phys. Rev. B **67**, 224105 (2003).
[12] T. Kakiuchi, Y. Wakabayashi, H. Sawa, T. Takahashi, and T. Nakamura, J. Phys. Soc. Jpn. **76**, 113702 (2007).
[13] Y. Tanaka and K. Yonemitsu, J. Phys. Soc. Jpn. **77**, 034708 (2008).
[14] N. Tajima, S. Sugawara, M. Tamura, Y. Nishio, and K. Kajita, J. Phys. Soc. Jpn. **75**, 051010 (2006).
[15] N. Tajima, S. Sugawara, M. Tamura, R. Kato, Y. Nishio, and K. Kajita, EPL **80**, 47002 (2007).
[16] K. Yamamoto, S. Iwai, S. Boyko, A. Kashiwazaki, F. Hiramatsu, C. Okabe, N. Nishi, and K. Yakushi, J. Phys. Soc. Jpn. **77**,

074709 (2008).
[17] K. Yakushi, H. Kanbara, H. Tajima, H. Kuroda, G. Saito, and T. Mori, Bull. Chem. Soc. Jpn. **60**, 4251 (1987).
[18] V. Zelezny, J. Petzelt, R. Swietlik, B. P. Gorshunov, A. A. Volkov, G. V. Kozlov, D. Schweitzer, and H. J. Keller, J. Phys. France **51**, 869 (1990).
[19] M. Dressel, G. Gruner, J. P. Pouget, A. Breining, and D. Schweitzer, J. Phys. I **4**, 579 (1994).
[20] P. Monceau, F. Nad, and S. Brazovskii, Phys. Rev. Lett. **86**, 4080 (2001).
[21] F. Nad, P. Monceau, and H. M. Yamamoto, J. Phys. C **18**, L509 (2006).
[22] H. Matsui, H. Tsuchiya, T. Suzuki, E. Negishi, and N. Toyota, Phys. Rev. B **68**, 155105 (2003).
[23] N. Tajima, J. Fujisawa, N. Naka, R. Kato, Y. Nishio, and K. Kajita, J. Phys. Soc. Jpn. **74**, 511 (2005).
[24] S. Iwai, K. Yamamoto, A. Kashiwazaki, F. Hiramatsu, H. Nakaya, Y. Kawakami, K. Yakushi, H. Okamoto, H. Mori, and Y. Nishio, Phys. Rev. Lett. **98**, 097402 (2007).
[25] S. Iwai, K. Yamamoto, F. Hiramatsu, H. Nakaya, Y. Kawakami, and K. Yakushi, Phys. Rev. B **77**, 125131 (2008).
[26] Y. Kawakami, S. Iwai, T. Fukatsu, M. Miura, N. Yoneyama, T. Sasaki, and N. Kobayashi, Phys. Rev. Lett. **103**, 066403 (2009).
[27] S. Miyashita, Y. Tanaka, S. Iwai, and K. Yonemitsu J. Phys. Soc. Jpn. **79**, 034708 (2010).
[28] K. I. Pokhodnia, A. Gragja, M. Weger, and D. Schweitzer, Z. Phys. B: Condens. Matter **90**, 127 (1993).
[29] K. Oshima, T. Mori, H. Inokuch, H. Urayama, H. Yamochi, and G. Saito, Phys. Rev. B **38**, 938 (1988).
[30] T. Sasaki, N. Yoneyama, and N. Kobayashi, Phys. Rev. B **77**, 054505 (2008).
[31] Photoinduced changes in $\sigma_1(\omega)$ and $\varepsilon_1(\omega)$ [$\Delta\sigma_1(\omega)$ and $\Delta\varepsilon_1(\omega)$] should be calculated from the THz time profile to determine changes in the electronic properties. However, it is difficult to obtain $\Delta\sigma_1(\omega)$ and $\Delta\varepsilon_1(\omega)$ because the phase shift in the THz time profile resulting from the PIMT is very small. This small photoinduced phase shift is attributable to the photoinduced HT state formed on the surface layer of thickness approximately 1 μm of the sample, reflecting the large difference between the penetration depth of the pump light (approximately 1.1 μm) and that of the THz probe ($\gg$the sample thickness of 50 μm). Therefore, we use the absorption change ΔOD to describe the changes in the electronic properties. As described later, $\Delta\sigma_1(\omega)$ at 20 K can be calculated using the multilayer model for the result at 20 K, as shown in the inset of Fig. 3(b).
[32] D. E. Aspnes, Thin Solid Films **89**, 249 (1982).
[33] T. Hanai, Kolloid-Z. **171**, 23 (1960).
[34] The Maxwell-Garnett equation should be applicable to the low-density guest particles in the host material. Therefore, ε_I and ε_M are exchanged for the high-density metallic region I although the original equation is valid for the low-density region III. For the intermediate region II, Hanai's equation[27] is used.
[35] P. C. Hohenberg and B. I. Hailerin, Rev. Mod. Phys. **49**, 435 (1977).
[36] M. P. Nightingale and H. W. J. Blote, Phys. Rev. Lett. **76**, 4548 (1996).
[37] Y. Tanaka, and K. Yonemitsu J. Phys. Soc. Jpn. **79**, 024712 (2010).